Materials Advances

ROYAL SOCIETY OF CHEMISTRY

PAPER

View Article Online
View Journal | View Issue

Cite this: *Mater. Adv.*, 2024, 5, 8986

Exploring the chemistry and composition of black soldier fly eumelanin, a material for a circular economy†

A. B. Mostert, *[a] S. Mattiello, [bc] S. Li, [d] G. Perna, [e] M. Lasalvia, [e] P. F. Ambrico, [b] J. V. Paulin, [f] J. V. M. Lima, [f] C. F. O. Graeff, [f] J. W. Phua, [g] M. Matta, [d] A. J. Surman, [d] R. Gunnella *[c] and M. Ambrico [b]

Received 14th August 2024,
Accepted 18th October 2024

DOI: 10.1039/d4ma00825a

rsc.li/materials-advances

Eumelanin is a black-brown biopigment that provides photoprotection and pigmentation in mammals, insects, and invertebrates. It can be obtained by oxidative polymerisation of 5,6-dihydroxyindole (DHI) and its 2-carboxylic acid (DHICA). Due to its unique physical and chemical properties and its biocompatibility, eumelanin is a promising biomaterial for applications in energy storage, biomedicine, and sensing. However, poor solubility in water and lack of sustainable and low-cost sources of eumelanin have so far limited the full exploitation of this biomaterial. Insect farming is rapidly emerging as an alternative source of eumelanin. Unlike other types of eumelanin, BSF eumelanin, which is extracted from the exoskeleton of the black soldier fly (BSF, *Hermetia illucens*), is water-dispersible; however, its fundamental chemical properties are not completely understood. Here, we report the characterisation of BSF eumelanin using various spectroscopy techniques. Contrary to what is known about other insect eumelanins, which are believed to contain exclusively DHI, our results indicate that BSF eumelanin may contain both DHI and DHICA moieties. We discuss the potential reasons for this discrepancy.

1. Introduction

Eumelanin is a black-brown biopigment that plays a crucial role as a protector from UV radiation damage and as a radical scavenger, and is also responsible for the dark pigmentation found in mammals, insects, and invertebrates. Eumelanin can be produced by oxidative polymerisation of two monomers, 5,6-dihydroxyindole (DHI) and 5,6-dihydroxyindole-2-carboxylic acid (DHICA) and their various redox and tautomeric states (Fig. 1).[1–4] While its structure is poorly understood, the material is considered a disordered oligomer system, with a hierarchical supramolecular structure characterised by π-stacking and hydrogen bonding interactions. The stacking distance can vary from ~3.2–4.0 Å depending on hydration and type of eumelanin.[5]

The ratio of DHI to DHICA determines the material's morphology and solubility, as well as its redox and radical scavenging activity.[6] For example, DHI-heavy eumelanin is more insoluble, likely as a consequence of a lower polarity and more efficient π-stacking, which prevents water from penetrating the aggregate structure.[7] In contrast, the presence of carboxylic acid

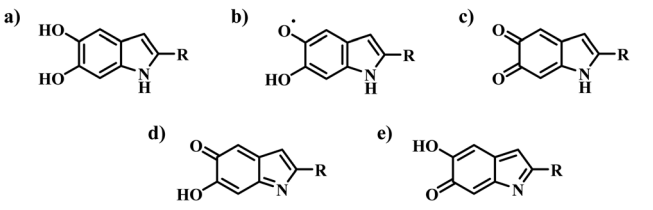

Fig. 1 The monomer building blocks of eumelanin. (a) 5,6-Dihydroxyindole (DHI) for R═H or 5,6-dihydroxyindole-2-carboxylic acid (DHICA) for R═COOH. (b) Protonated semiquinone. (c) Quinone. (d) Quinone imine tautomer. (e) Quinone methide tautomer.

[a] *Department of Physics and Centre for Integrative Semiconductor Materials, Swansea University Bay Campus, Fabian Way, Swansea, SA1 8EN, UK. E-mail: a.b.mostert@swansea.ac.uk*
[b] *CNR-Institute for Plasma Science and Technology, Bari Branch, Via Amendola 122/D, I-70125 Bari, Italy*
[c] *School of Science and Technology University of Camerino, Via Madonna delle Carceri 9, I-62032, Camerino, Italy. E-mail: roberto.gunnella@unicam.it*
[d] *Department of Chemistry, King's College London, Britannia House, 7 Trinity Street, SE1 1DB London, UK*
[e] *Department of Clinical and Experimental Medicine, Università degli Studi di Foggia Via Napoli 20, I-71122 Foggia, Italy*
[f] *São Paulo State University (UNESP), School of Sciences, Department of Physics and Meteorology, Bauru/SP, Brazil*
[g] *Insectta Pte. Ltd., 8 Cleantech Loop, S637145, Singapore*

† Electronic supplementary information (ESI) available. See DOI: https://doi.org/10.1039/d4ma00825a

groups in DHICA prevents the tight π-stacking of aggregates, making the material more accessible to water permeation.[6] Notably, naturally sourced eumelanin tends to be more DHICA-rich compared to its synthetically made variants.[3]

Eumelanin is of great interest due to its unique physical and chemical properties,[1,2,8] which are uncommon in bioderived, and potentially biocompatible, materials. For example, eumelanin has a broad-band optical absorbance,[9,10] can chelate metal ions in large quantities,[11–18] exhibits paramagnetism,[12,17,19–24] serves as radiation protection,[25,26] binds pharmacological products,[27–29] presents photoconductivity,[30–32] has redox activity,[33–36] and has humidity dependent conductivity,[10,11,18,31,32,37–44] to name just a few key properties. A number of applications exploiting these properties have been reported, *e.g.*, pH sensing,[45–47] transistor devices,[11,45,48,49] capacitors,[50] battery components,[33,51–53] water filtration,[54] and optical coatings.[55]

Even though eumelanin has had the potential to be a "work horse" biomaterial, it has historically had four major drawbacks:

(1) It is not readily sourced at large scale

Eumelanin extracted from cuttlefish (*Sepia officinalis*) ink sacs has been characterised extensively and incorporated in proof of-concept applications.[56,57] However, this sourcing approach is neither scalable nor sustainable. The synthesis of eumelanin by oxidative polymerisation of its precursors[1] is another common strategy; however, it is not cost-effective; synthetic eumelanin and its building blocks (DHI and DHICA) are prohibitively expensive. Overall, neither approach abides by the ideals of a circular economy.

(2) It is not readily processed

Eumelanin is notoriously insoluble in water and common solvents.[1–3] To enhance solubility, or at least obtain a fine dispersion, it is possible to use DMSO as a solvent during synthesis,[58] or alternatively to synthesize under O_2 pressure.[59] Alternatively, eumelanin can be synthetically modified post-synthesis to increase solubility.[60] However, these examples run counter to a circular economy framework due to the solvent or reagent requirements.

(3) It is not chemically/morphologically well-defined

Eumelanin is a heterogeneous 'polymer' that lacks a well-defined chemical structure (the lack of solubility, and crystallinity is an important contributing factor in this). Eumelanin from different organisms or obtained *via* different synthesis methods/precursors have different properties,[3] which are expected to impact its processability, functionalisation and application.[1] This lack of "standardisation", and means to standardise, present a challenge.

(4) Its research community is fragmented

The melanin research community is very diverse, but fragmented across research 'silos': medicine, biology/biotechnology, paleontology, materials science, chemistry.[61] Furthermore, the interests of these groups often do not intersect, with research focused either on melanin nanoparticles and their applications or on melanogenesis and small oligomeric precursors.[61]

Due to the issues above, eumelanin has not received widespread attention and remains a niche material. This is perhaps set to change: the growing industry of insect farming is emerging as a source of sustainable, abundant and low-cost eumelanin, offering a solution to points (1) and (2).

Insect farming is on the rise as a solution to the issues of protein scarcity and food security; by manufacturing an alternative animal feed while valorising food waste, it fulfils a circular economy framework.[62,63] The black soldier fly (BSF, *Hermetia illucens*) is the most popular insect for this endeavour due to its rapid reproduction cycle and low carbon footprint.[64–68] From BSF farming, high-value products, such as chitin and eumelanin, can be extracted; the latter will be referred to as BSF eumelanin henceforth.[69–71] BSF eumelanin offers unique properties that set it aside from other types of eumelanin, most notably that it is *water-dispersible*.[65,69–71] Furthermore, given that only a single species is involved, one may expect a material with consistent properties. In this work, we set out to explore the chemical composition of BSF eumelanin in more detail; we hope our study will spur further research and future device applications for this 'new' kind of eumelanin.

2. Materials and methods

2.1. Eumelanin extraction

BSF eumelanin powders were provided by the manufacturer Insectta Pte. Ltd for research purposes. The material is produced *via* a patented targeted extraction process from the black soldier fly (*Hermetia illucens*).[69,70]

In brief, pupal exuviae were homogenised into ~0.5 mm pieces and demineralised with 10% (w/w) lactic acid for 3 h at 25 °C. The solid fraction was deproteinated with 1 M sodium hydroxide for 3 h at 50 °C. Following this, BSF eumelanin was liberated from the solid fraction by heating with 2 M sodium hydroxide for 3 h at 90 °C. The pH of the supernatant was corrected to 1 with 37% (v/v) hydrochloric acid to precipitate BSF eumelanin, which was collected by centrifugation and further subjected to a series of proprietary steps in order to derive a lyophilised, salt-free, water-dispersible powder (Note: we refer to stable dispersions of these particles here as 'solution' for clarity). The latter property is achieved at pH 7.3, lower than a standard synthesis pH of 8.[3]

Generally, as part of the preparation of the material, the manufacturer recommends filtering, to ensure that any minor insoluble fraction is removed. This study predominantly applies this approach, but some important experimental results will be highlighted where the unfiltered material is also tested for contrast.

2.2. Thin film deposition

Solutions of BSF eumelanin were prepared by stirring in deionized water at a concentration of 20 mg mL^{-1}. Thin films

were prepared from approximately 10 μL of the solution *via* drop casting deposition and left to dry in a fume hood at room temperature for several hours.

For atomic force microscopy (AFM) and Raman measurement, drop casting was done on an FTO glass substrate (Sigma-Aldrich). For X-ray Photoelectron Spectroscopy (XPS), a Si(001) substrate after 0.1% HF solution etching of the oxide was used, and subsequently metallized by 5 nm Cr deposition. BSF eumelanin 10 mg mL^{-1} solution was filtered by a 0.45 μm filter (Millipore) to remove possible residues.

For UV-Vis, both filtered and unfiltered solutions, were drop cast onto UV-ozone treated (Ossila Ltd, 5 min) and untreated glass substrates.

2.3. UV-Visible techniques

Absorbance spectra (100 nm to 3500 nm) for solutions of filtered (0.2 μm and 0.45 μm filters, Millipore) and unfiltered material were performed with a Lambda 40 PerkinElmer UV-Vis spectrophotometer (Waltham, MA, USA). Solutions contained 2 mg mL^{-1} BSF eumelanin dispersed in distilled water. The samples were examined in quartz cuvettes with an optical path of 1 cm.

For thin films of material, transmission and reflectance spectra were obtained using a 150 mm diameter integrating sphere coupled to a Lambda 950 UV-Vis-NIR spectrometer (PerkinElmer). We employed a wavelength λ range between 2000 and 350 nm with a wavelength step of 10 nm and used an InGaAs detector. An individual slide was measured four times, with each measurement being taken at a 90-degree rotation of the slide to the previous measurement. Data was then averaged to obtain a representative spectrum for the slide. Absorbance spectra was obtained *via* the relation $A = 100\% - T - R$ where A is the absorbance, T is the transmission and R is the reflectance. The transmission data was then further analysed using NKFinder from which the attenuation coefficient k was obtained and then the absorption coefficient $\alpha = \frac{4\pi k}{\lambda}$ calculated.[72] We note that for the modelling we derived a function for R derived from the transmission in the Cauchy regime as inputting the reflection data gave unphysical results.

2.4. Morphological analyses

Atomic force microscopy (AFM) images were acquired in tapping mode by using a CSI Nano-observer and P-doped n-type Si cantilever (resonance frequency = 75 kHz). The measurements were performed by using resonant mode. Gwyddion software was used for the processing of the images.[73] The calculation of the average particles size was carried out using ImageJ software by measuring the length and determining the average size.[74]

2.5. DLS and zeta potential for particle size and surface charge analysis

Dynamic light scattering (DLS) and zeta potential measurements of BSF eumelanin particles in H_2O solution were performed using a Litesizer DLS 500, DLS particle size and zeta potential analyzer (Anton Paar Ltd, UK) for the determination of the particle size distributions and zeta potential of dispersed BSF eumelanin particles in water, at room temperature (*ca.* 25 °C). For measurements, the automatic angle selection setting (Anton Paar Kalliope) was used. Fisherbrand™ disposable cuvettes (Fisher Scientific, UK) were used to perform DLS measurements. Measurement cuvettes (Omega Mat. No. 225288, Anton Paar Ltd, UK) were used to perform zeta potential measurements. Briefly, 0.5 mg mL^{-1} of BSF eumelanin solution was prepared and filtered using Fisherbrand™ PTFE Syringe Filter 0.2 μm pore size, the sample was measured in quadruplicate for DLS scattering and a single time for zeta potential. Zeta potential distributions were normalised and fit to Gaussian functions using Origin 2020.

2.6. FTIR and Raman techniques

Attenuated total reflection Fourier-transform infrared spectroscopy (ATR-FTIR) was recorded on BSF eumelanin powder from 4000 to 600 cm^{-1} with a PerkinElmer Spectrum 100 FT-IR instrument (Waltham, MA, USA) by total reflectance on a CdSe crystal. To obtain more information about vibration modes we performed an analysis using Voigt functions (convolution of Gaussian and Lorentzian functions in a ratio of 20% of Lorentzian and 80% of Gaussian) with Fityk (version 1.3.1).

Additional Raman analyses were performed on a BSF eumelanin thin film on a FTO glass substrate using a HORIBA IHR320 micro-Raman Scattering system (Horiba, Palaiseau, France) equipped with an optical Microscope model Olympus BXF41 (with 5×, 20×, 50×, 100× objectives) (Münster, Germany). The Raman spectrometer was operated at 532 nm (diode laser). To obtain information about the melanin components, the spectrum was fitted into a set of Gaussian functions using Fityk (version 1.3.1).

2.7. XPS measurements

The X-ray photoelectron spectroscopy (XPS) measurements were performed using Al-Kα un-monochromatised sources) (PSP Vacuum Technology) and hemispherical analyser VG-Clam 4.

The modelling of the data was performed using Fityk (version 1.3.1) using a subtraction of a linear background and a pseudo-Voigt profile for the peaks utilising mixed Gaussian/Lorentzian with 20% Lorentzian weighting.

The sensitivity factor library used from theoretical photoelectron cross-section specific for Mg/Al-Kα sources used CASA-XPS code.[75]

Surface scans on eumelanin like materials are generally good enough to give indications of the bulk elemental composition. For thin film morphologies the exact chemical nature of the surface and the bulk can be considered equivalent.[76]

2.8. HPLC measurements

An alkaline hydrogen peroxide oxidation (AHPO) analysis was performed to enable observation of the distribution of oxidation products from eumelanin materials, following procedures reported by Ito *et al.*[77,78] Briefly, the samples were 'digested' using AHPO and high performance liquid chromatography

(HPLC) analysis was used to determine the concentration of ''markers'' of oxidised eumelanin products.

Any filtration was performed using Fisherbrand™ PTFE Syringe Filter 0.2 μm pore size. 2.5 mg of extracted eumelanin was dispersed in 1 mL of H_2O; the solution was slowly filtered through the 0.2 μm syringe filter described above. After filtration the syringe filter was purged with an additional 1 mL of H_2O; the combined 2 mL solution was subjected to lyophilization to obtain a filtered BSF eumelanin solid.

AHPO. In a 2 mL Eppendorf tube, 2.5 mg of eumelanin was subjected to 100 μL of water and 375 μL 1M K_2CO_3 (Fisher Scientific, UK) and 25 μL 30% H_2O_2 (Sigma Aldrich, UK) were added. The Eppendorf tube was stirred at room temperature using an SciQuip rotator for 20 hours. The remaining H_2O_2 was quenched with 50 μL Na_2SO_3 (Fisher Scientific, UK) and acidified to pH 1 using 150 μL 6 M H_3PO_4 (Thermo Scientific, UK). The reaction mixture was centrifuged, and 30 μL of supernatant was directly analysed by HPLC. Acid hydrolysis of BSF eumelanin was performed as described in Ito *et al.*[77] with a minor modification. Briefly, acid hydrolysis was performed on 2.5 mg BSF eumelanin suspended in 1 mL 6 M HCl in a vial and heated at 110 °C for 16 h. The solution was then diluted with 1 mL of water and centrifuged. The suspension was collected and subjected to the AHPO process. Each digestion was performed in duplicate, with each sample measured in duplicate.

Synthesis of ''markers''. Pyrrole-2,3-dicarboxylic acid (PDCA) and pyrrole-2,3,5-tricarboxylic acid (PTCA) were synthesised according to reported methods by Ito and Wakamatsu with minor modifications.[79] ^{1}H NMR of PDCA: (400 MHz, MeOD) δ 7.05 (s, 1H), 6.81 (s, 1H). ^{1}H NMR of PTCA: (400 MHz, MeOD) δ 7.34 (s, 1H). Thiazole-2,4,5-tricarboxylic acid (TTCA) was synthesised according to reported methods by M. d'Ischia *et al.* with minor modifications.[3] ^{13}C NMR of TTCA: (101 MHz, D_2O) δ 171.31, 167.55, 165.78, 165.14, 153.32, 136.12. See ESI† for further spectra, demonstrating purity.

HPLC. HPLC measurements were performed using the Agilent 1100 series HPLC. A reversed phase C18 column (Poroshell 120 EC-C18; 4 μm; 4.6 × 250 mm) from Agilent technologies, with a Diode Array detector measuring absorbance at 288 nm. The mobile phase was 0.1 M potassium phosphate buffer (Sigma Aldrich, UK), pH 2.8, containing 1 mM TBA^+Br^- (Fluorochem, UK): methanol at 83 : 17 (v/v) and a flow rate of 0.5 mL min^{-1} and analyses were performed at 45 °C. The markers were used to calibrate measurements of marker concentration in eumelanin samples (see ESI† for calibration curves), with peaks identified by comparing retention times. All solvents were purchased from Sigma Aldrich, UK (HPLC grade).

2.9. NMR measurements

^{13}C CP/MAS analyses were performed on a Bruker Avance III 400 MHz spectrometer equipped with a 4 mm CP/MAS probe, operating at 100.5 MHz for ^{13}C. The ^{13}C CP/MAS spectra of the solid eumelanins were obtained by means of the cross-polarization technique (Cross-Polarization Magic Angle Spinning – CPMAS) with contact time of 3 ms, repetition time of 2 s and MAS rotation frequency of 5 kHz. Two pulse phase Modulation (tppm) proton decoupling was used.

Two eumelanin materials were employed for comparison. The first was an unfiltered BSF eumelanin, and the other for control, was a synthetic eumelanin. The latter was synthesized from 1 g of 3,4-dihydroxy-phenyl-DL-alanine (DL-DOPA; Sigma-Aldrich, ≥98%), which was dissolved in 200 mL of MiliQ water (18 MΩ cm). The mixture's pH was adjusted to be between 8 and 10 by the addition of 1.4 mL of ammonium hydroxide (NH_4OH; synth, 28–30%). The solution was stirred at room temperature (27 °C) and oxygenated using an air pump for three days. For extraction and purification, a 3500 MWCO dialysis membrane was used with MiliQ water as a dialysate medium, which was changed for six days until no further colour change was observed. Finally, drying the aggregated solution was done in an oven at 90 °C for two days.

2.10. Elemental analysis

CHNS analyses were performed by the Elemental Analysis Laboratory, Department of Chemistry, Faculty of Science, National University of Singapore using a ThermoFisher Scientific FlashSmart Elemental Analyser, which operates with dynamic flash combustion of the sample. The instrument is calibrated for CHNS with sulfanilamide standard, using the *K* factor as the calibration method. Samples were weighed into tin containers and introduced into the combustion reactor *via* an autosampler with oxygen. After the combustion, the analyte gases are carried along a helium flow to a layer containing copper, then swept through a GC column, which provides the separation of the combustion gases and are detected by a thermal conductivity detector. The limit of detection for the instrument is 100 ppm or 0.01% w/w.

3. Results and discussions

3.1. UV-Visible spectroscopy

The broad-spectrum absorbance of eumelanins is its most defining feature. Fig. 2 shows the UV-Vis spectra for a BSF eumelanin suspension (filtered with a 0.45 μm filter, a 0.22 μm filter). The spectra exhibit a broad-band, exponential decay, expected of eumelanin, though with a peak at around 280 nm (*vide infra*).[2,9,80] Overall, the solution spectra indicates that the BSF eumelanin optical response is typical of eumelanins.

In previous reports, several attempts were made to interrogate the absorbance spectra to give quantitative insight into eumelanin compositions (an approach also adopted for insect eumelanins).[85] In particular, the ratio of absorbance at 650 nm and 500 nm (A_{650}/A_{500}) has been considered to estimate eumelanin/pheomelanin content,[86–88] and in the absence of pheomelanin, as a value enabling the estimate of the DHI/DHICA content (for example in human hair).[89] Given that our elemental analysis (see ESI†) and elemental XPS (*vide infra*) detect no sulfur present, and we do not observe significant amounts of the TTCA marker on AHPO-HPLC analysis (see ESI†) or pheomelanin-related peaks in FTIR & Raman spectroscopy (*vide infra*), we

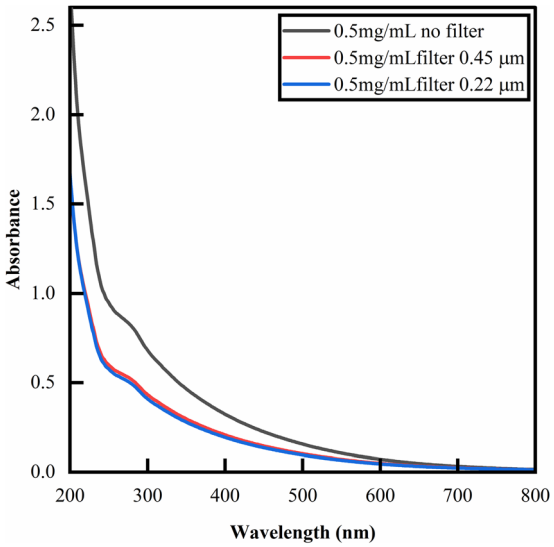

Fig. 2 UV-Vis absorbance of BSF eumelanin suspensions at 0.5 mg mL^{-1} in deionised water. The spectrum is that of an exponential decay, commonly observed for eumelanins,[9] but exhibiting a peak at 280 nm that is likely due to additional proteins in the material.[81–84] Filtration state indicated in the figure.

discount significant presence of pheomelanin. Thus, in principle, A_{650}/A_{500} ratio analysis could be pertinent to a DHI/DHICA analysis. However, the A_{650}/A_{500} ratios reported in the literature (see Fig. S7, ESI†) do not provide a sufficient basis for estimation. Considering this, we refrain from drawing quantitative conclusions, but report A_{650}/A_{500} ratios for BSF eumelanin (0.3, unfiltered; 0.33 filtered), noting that these values fall into the range reported for mixed DHI/DHICA eumelanins.[82–84,90,91]

Turning to thin films, we observe a representative set of transmission, reflectance, and absorbance optical data, as well as the corresponding absorption coefficient spectrum, in Fig. 3. The overall absorbance profile shows the same behaviour as observed in solution: decaying exponential behaviour with increasing wavelength, consistent with other eumelanin thin films.[10] An attempt was made at an A_{650}/A_{500} ratio analysis for this thin film data (see ESI†); however, the A_{650}/A_{500} ratio fall outside the ranges observed in solution, and we conclude performing this analysis in the solid state is not comparable.

3.2. Morphology

The morphology of BSF eumelanin thin film presents a surface characterized by spherical particles with an average diameter of 140 ± 40 nm (Fig. 4a and c), similar to previous reports on natural eumelanin obtained from *Sepia* ink.[92,93] The surface profile suggests roughness, as estimated by the range of about 10 nm (Fig. 4b).

DLS analysis of a BSF eumelanin dispersion observed very similar particle diameters as seen in AFM, ranging from 130–159 nm, with an average measurement of *ca.* 145 nm (Fig. 5a).

Using the same instrument, the surface (zeta) potential of BSF eumelanin particles was measured as *ca.* −66 mV (Fig. 5b). This is a significantly negative charge and is consistent with the presence of carboxylate groups at the particle surface, providing some explanation for BSF eumelanin particles being readily dispersed in water.

3.3. Raman and ATR-FTIR results

The Raman spectrum of BSF eumelanin is depicted in Fig. 6a. The data show two wide bands centred around 1350 cm^{-1} and 1550 cm^{-1}. These two dominant bands are similar to other reports on eumelanin elsewhere, where the two peaks tend to show a range of values (1335–1415 cm^{-1} and 1528–1600 cm^{-1}), with exact values depending on the laser excitation wavelength, the broadness of the peaks and the origin of the sample.[94–98] The blue curve shows the spectrum of the FTO substrate analysed with the same laser wavelength as the BSF eumelanin thin film. Spectra were fitted by using Gaussian functions, with the assignment of the Raman bands done with the use of previous literature (see Table 1).

The ATR-FTIR spectrum of BSF eumelanin is shown in Fig. 6b. The fitting analysis of the spectra used Voight functions

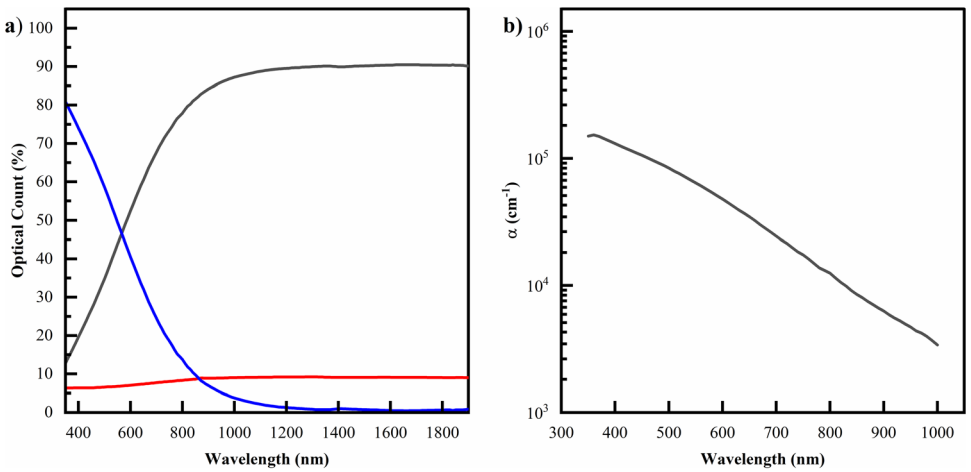

Fig. 3 (a) The optical data for samples of a filtered solution drop cast on UV-ozone treated glass. (b) The corresponding modelled absorption coefficient. Datasets for the other permutations of (un)filtered and (un)treated films can be seen in the ESI.†

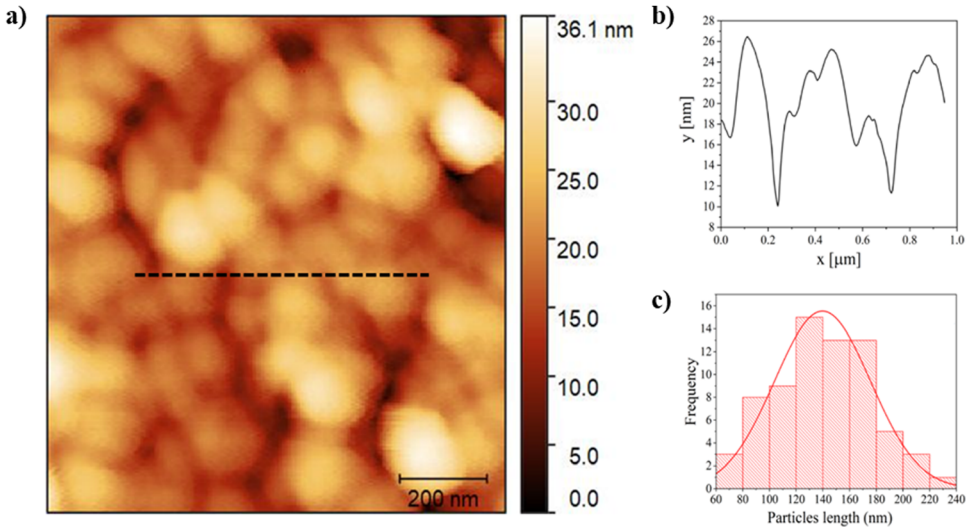

Fig. 4 (a) AFM image of a BSF eumelanin film. The black line indicates the line position of the profile capture depicted in (b). (b) A 1D AFM profile scan of the film surface. (c) A histogram of particle dimensions with an associated distribution curve.

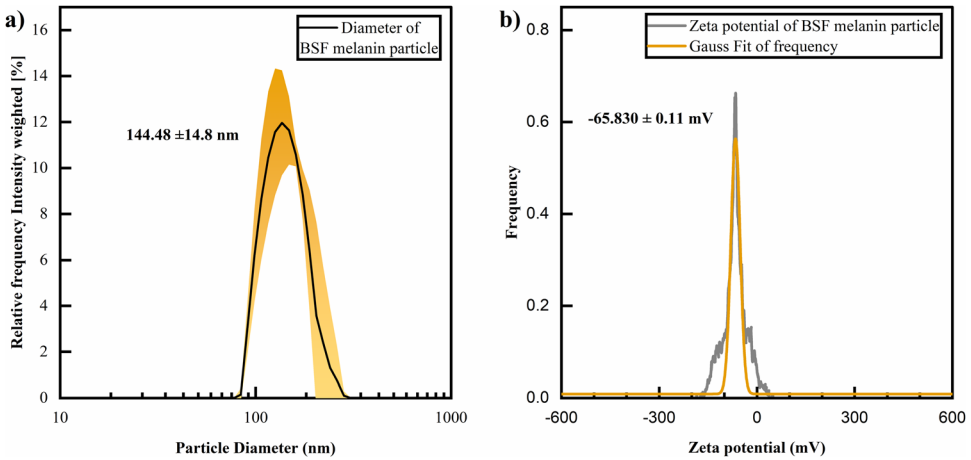

Fig. 5 (a) Size distribution of dispersed BSF eumelanin particles determined by measuring diameters in dynamic light scattering (DLS). The standard deviation of 4 measurements determined the confidence region. (b) Zeta potential analysis of BSF eumelanin particle.

(grey lines, Fig. 6b), with assignments of the vibrational peaks/modes based on previous works, and recorded in Table 1.

Both the Raman and FTIR spectra for BSF eumelanin are consistent with a typical eumelanin polymer. Of specific interest are the vibrational modes at 1714 cm^{-1} (Raman) and 1214 cm^{-1} (FTIR) as these modes are typical of DHICA group vibrations and support our observations of the presence of DHICA. However, since the relationship between FTIR and Raman line strengths and DHI/DHICA concentrations are not established, we can only conclude that DHICA is present.

Furthermore, the FTIR and Raman spectra do not show peaks related to the presence of pheomelanin. In particular, the FTIR signal of pheomelanin presents a peak related to the vibration of the S–O bond at 1172 cm^{-1},[99] which is absent in the spectra acquired on eumelanin from black soldier flies. At the same time, the Raman spectrum (Fig. S8, ESI†) also does not present the peaks related to pheomelanin at 500 cm^{-1} and the single band at 1490 cm^{-1}.[100] The data therefore support the absence of pheomelanin.

3.4. XPS analysis

XPS has been established to obtain the elemental composition of eumelanins, with literature demonstrating that elemental analysis by surface scans of the material is equivalent to the bulk elemental composition.[76] Fig. 7a depicts an example of a wide survey XPS spectrum of a filtered BSF eumelanin film and indicates the presence of C, O, N and Na 1s core levels. The presence of Na at 1080 eV is likely due to the precipitation method used during the material extraction process. Also, minimal traces of Cr are visible while S traces are not visible within the sensitivity of the XPS spectrometer.

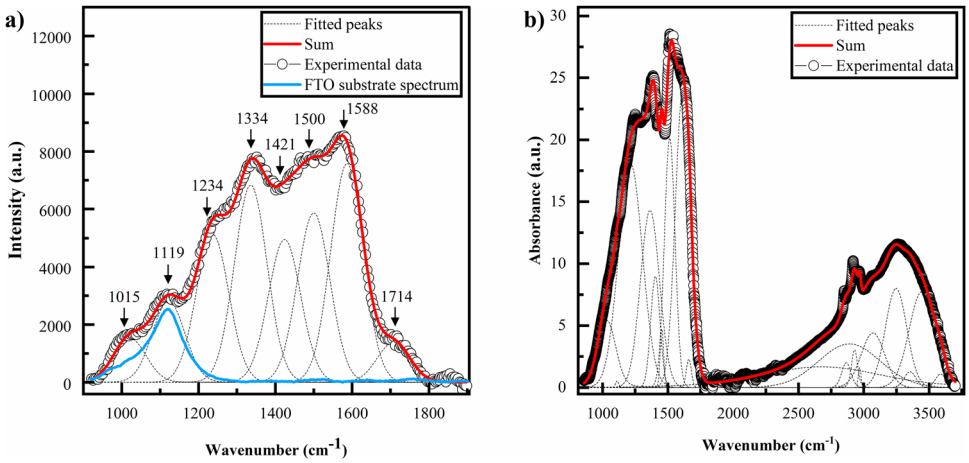

Fig. 6 (a) Raman spectra of a drop cast film of BSF eumelanin deposited on a FTO substrate. Grey lines indicate the fitted peaks and the blue curve the FTO substrate spectrum. (b) FTIR spectrum of BSF eumelanin powder sample. The assignments of the fitted peaks are listed in Table 1.

Table 1 Peak assignment of FTIR and Raman spectra for BSF eumelanin and the literature used

Peak position in fit, IR (cm^{-1})	Peak position in fit, Raman (cm^{-1})	Current assignment	Ref.
	1015	C–H plane deformation	Centeno *et al.*[94]
1033		δ(CH) + δ(NH) + ν(C–O)	Bedran *et al.*[98]
1111		δ(CH) + δ(NH) + ν(C–O)	Bedran *et al.*[98]
	1119	-FTO substrate	Measured (Fig. 6)
1214		δ(OH) + δ(CH) + ν(C(O)–OH in carboxyls) + ν(C–OH inconjugated cycles)	Bedran *et al.*[98]
	1234	ν(CO) + δ(CH) + δ ring	Roldan *et al.*[95]
	1334	ν(CN) + δ(OH) + ν ring	Roldan *et al.*[95]
1363		ν(CN) + δ(OH) + ν(ring)	Bedran *et al.*[98]
1404		Cycle semiquinone C⁼O stretching	Bedran *et al.*[98]
	1421	δ(OH) + ν ring or C–C, C–N in-plane vibration in pyrrole	Roldan *et al.*[95] & Perna *et al.*[97]
1454		semiquinone C⁼O stretching	Beldran *et al.*[98]
	1500	C=N in semiquinone/NH bending	Centeno *et al.*[94]
1514		ν(ring) + δ(NH) + δ(CH) or Semiquinone anion C⁼O stretching	Bedran *et al.*[98]
	1588	Indole ring vibration	Perna *et al.*[97]
1614		ν(ring) + ν(C=O)	Bedran *et al.*[98]
	1714	C=O stretching in COOH	Perna *et al.*[97] & Perna *et al.*[96]
2675		Enol H-bonded OH stretching	Bedran *et al.*[98]
2866		Aliphatic C–H stretching	Bedran *et al.*[98]
2929		Aliphatic C–H stretching	Bedran *et al.*[98]
2968		Aliphatic C–H stretching	Bedran *et al.*[98]
3070		Aromatic C–H stretching	Bedran *et al.*[98]
3247		ν(NH) in aromatic system	Bedran *et al.*[98]
3354		ν(C(O)O–H) hydrogen bonded	Bedran *et al.*[98]
3444		OH H-bonded stretching in water	Bedran *et al.*[98]
3588		OH stretching in water	Bedran *et al.*[98]

To understand the chemical structure of the BSF eumelanin in greater detail, we performed additional fitting of the high-resolution scans to the C1s core level data (Fig. 7b). A fit was obtained using Voigt functions of 0.80 eV and 0.15 eV, respectively, for Gaussian and Lorentzian HWHM. The C1s spectrum can be decomposed into four chemically shifted components with characteristic binding energy values: at 284.6 eV consistent with a C=C/C–C bond (58%); at 286.0 eV consistent with a C–N and/or C–O bond (24%), at 287.8 eV consistent with C=O/C–O bonds (16%); which is in line with other systematic XPS work on synthetic eumelanin systems.[76,101] Finally, a minor component related to COOH group is found at 289.5 eV (2%). The ratio of C–C : C–O(N) : C=O is 58 : 40 : 2, intermediate between that of DHI (67 : 33 : 0) and DHICA (60 : 33 : 7).

An important aspect of the XPS data is the elemental analysis. By comparing the peak areas of C, N and O 1s, core levels, after the subtraction of the background, and adjusting for the sensitivity factors, it is possible to estimate the ratio between the elements composing the samples. In Table 2, the atomic composition (%) that is obtained for the BSF eumelanin film can be compared to theoretical values for DHI and DHICA. As can be seen, the atomic percentages are intermediate between expected DHI and DHICA, indicating a probable DHICA component.

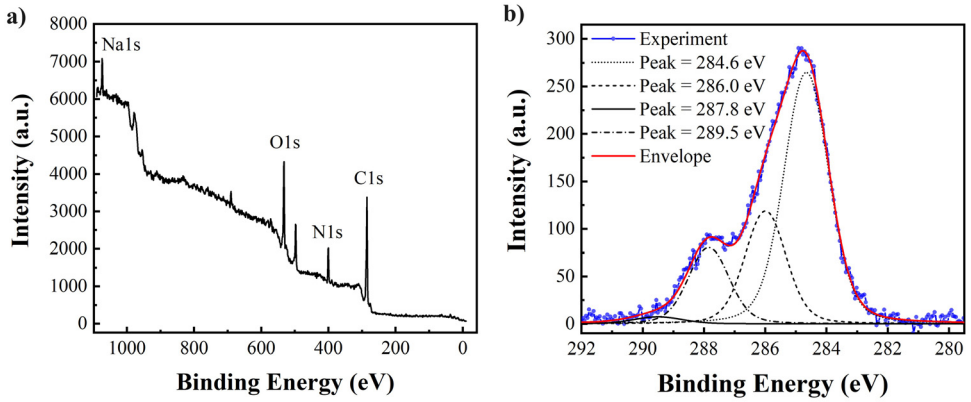

Fig. 7 (a) The XPS wide survey scan. (b) High-resolution C1s core level spectrum of thin film BSF eumelanin with fitting.

Overall, the high-resolution fitting and elemental analysis indicates a material consistent with the composition of DHI and DHICA.

3.5. HPLC

While eumelanin is not typically soluble, the oxidation of eumelanin materials (using hydrogen peroxide) to observe oxidation products (''markers'') by HPLC has been established over many years.[77,79] The balance between the PDCA and PTCA markers is thought to reflect the balance between DHI and DHICA content in eumelanin materials.[102] We produced the requisite markers and implemented this method, as reported by Ito *et al.* (see Methods and ESI†).[79]

Performing AHPO on BSF eumelanin, we observe product chromatograms like those previously reported for eumelanin samples (Fig. 8). For native BSF eumelanin, a PDCA/PTCA (w/w) ratio in of *ca.* 0.22 is observed (see Fig. 9, and ESI† for data). This ratio is not altered dramatically either by filtration or HCl-treatment. The latter is expected to remove proteins and low molecular weight components from eumelanin samples, suggesting this reflects the bulk structure of the material, rather than surface contamination (indeed the ratio drops slightly following this treatment, consistent with a higher % DHICA). This PDCA/PTCA ratio is somewhat smaller than other insect eumelanins reported by Ito *et al.*,[102] consistent with the presence of DHICA in BSF eumelanin (this would be estimated around 20%, using published AHPO calibration data, though we note that scant data in this range precludes confident quantification.[89,103]

Ratios between PDCA and TTCA can be used to estimate pheomelanin content.[104] We note that comparison with TTCA standards shows no/negligible TTCA detected in BSF eumelanin (see ESI,† Fig. S12–S15 for the data). This further supports the conclusions we draw from elemental analyses and FTIR/Raman spectroscopies on the absence of detectable levels of pheomelanin.

Table 2 Atomic concentration in samples BSF eumelanin film as determined from XPS and the respective theoretical values of DHI and DHICA

Element	% AT BSF melanin	DHI	DHICA
C	0.66 (2)	0.73	0.64
N	0.11(2)	0.09	0.07
O	0.23(2)	0.18	0.29

3.6. NMR results

Fig. 10 shows the ^{13}C CP/MAS NMR of BSF eumelanin in comparison to synthetic eumelanin. As expected, the spectra have broad resonances due to the heterogeneous nature of eumelanin. These signals can be divided into three central resonance regions: (I) 0–90 ppm, designated to aliphatic groups; (II) 95–155 ppm, due to aromatics carbons from pyrrole and indole carbons; and (III) 160–200 ppm, related to carboxyl and quinone groups.

Synthetic eumelanin gives a weaker region I signal due to the uncyclized precursor DL-DOPA, which can imply that the intense signals found in the aliphatic region of BSF eumelanin are primarily due to residual protein components and environmental impurities from the biological medium. Such behavior is compatible with other examples of natural melanin.[105–108] We note that S. Ghiani *et al.* attributed a combination of eumelanin and protein to the highly intense signal of the carboxyl region.[106]

A theoretical prediction using the incremental method of the ChemDraw Ultra (version 12.0.2) software package for each peak assignment is shown in the ESI† (Fig. S16).[109] Based on the predictions, the main contribution of eumelanin should be the aromatic signal, and we can try a qualitative comparison between BSF eumelanin and the DL-DOPA synthetic eumelanin, the latter of which is well known to be relatively poor in DHICA content ($\sim$5–10%).[3]

The CP/MAS experiment can differ between samples due to proton concentration and relaxation rates. Assuming that the amount of ^{13}C nuclei is equal in both samples, we could expect BSF eumelanin to have an extensive cross-linking between the DHI/DHICA units and DHI/DHICA and protein. This would reduce the proton concentration and yield the low intensity of the aromatic region.

The aromatic-to-carboxyl signal area ratio is usually employed to compare eumelanin content in a given sample.

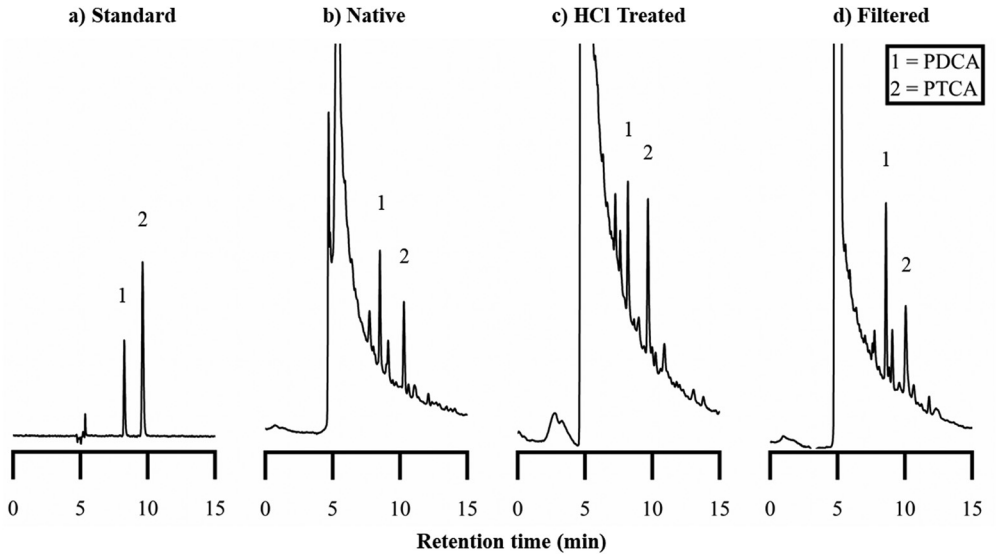

Fig. 8 High-performance liquid chromatography (HPLC) chromatograms of (a) standard eumelanin markers, and AHPO mixtures from (b) original native BSF eumelanin, (c) HCl–AHPO mixtures from BSF eumelanin and (d) AHPO mixtures from 0.2 μm filtered BSF eumelanin.

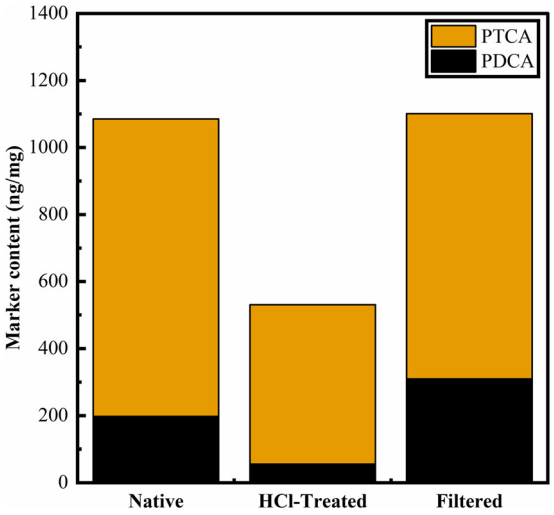

Fig. 9 Marker content observed in AHPO mixture of BSF-Mel (ng mg^{-1}).

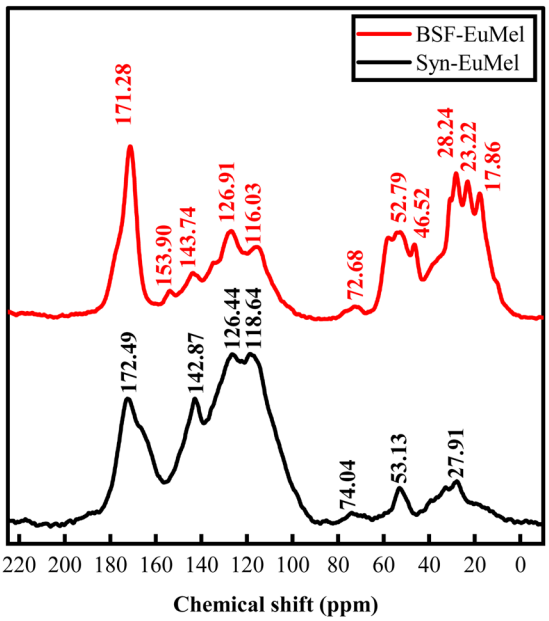

Fig. 10 ^{13}C CP/Mas NMR spectra of BSF eumelanin (top, BSF-EuMel) and synthetic eumelanin (bottom, Syn-EuMel).

Thus, one would expect a low concentration of eumelanin in BSF eumelanin compared to synthetic eumelanin by a factor of approximately 2, as indicated by Table 3 (see R-II/R-III). Indeed, the abundance in BSF eumelanin of the protein matrix is such that the signal around 154 ppm is seen in Fig. 10[106,108] and is aligned with purity ranging from 40 to 80%.[69]

To compare the DHI/DHICA units between BSF eumelanin and synthetic eumelanin, we normalise the aromatic and carboxyl region area to the eumelanin content. The data is reported in Table 4. The BSF eumelanin has a decrease in the aromatic region and an increase in the carboxyl region. This behavior has been linked to the rise in the DHICA ratio and to the oxidation of phenolic carbons.[59,105] Interestingly, the increase in oxidation is compatible with previous reports on BSF eumelanin.[70]

3.7. Discussion

The synthesis of eumelanin in higher animals is quite well understood. Briefly, both tyrosine and L-3,4-dihydroxyphenylalanine (L-DOPA) are oxidised *via* catalysis by the enzyme tyrosinase into dopaquinone. After catalysis, non-enzymatic intramolecular cyclization occurs leading to dopachrome, which in turn is then converted to DHICA by tyrosinase-related protein or dopachrome isomerase. In contrast, DHI is formed non-enzymatically.[77,102,110,111] However, work by Barek *et al.* investigated a number of insects and found that the

Table 3 Normalised signal (to total signal) areas in ^{13}C CP/MAS NMR spectra

Sample	Aliphatic (0–85 ppm)	Aromatic A (95–140 ppm)	Aromatic B (140–155 ppm)	Carboxyl (160–190 ppm)	R-II/R-III ratio
BSF eumelanin	0.49	0.23	0.06	0.19	1.53
Synthetic eumelanin	0.12	0.52	0.16	0.21	3.24

eumelanin formed was based on DHI only, formed from dopamine.[102] It is noted that thus far no DHICA-producing enzyme has been characterised in insects.[112] This led Sugumaran and Barek, in their extensive overview, to suggest that the question "*Do insects and other arthropods make significant amounts of pheomelanin and DHICA melanin?*" is unresolved, and note: "*. . .in insect systems the presence or absence of DHICA melanin should be unequivocally assessed*".[112] Given this background, the presumption coming into the present study was that BSF eumelanin would be a solely DHI-based eumelanin.

However:

(1) We see no evidence of significant pheomelanin fractions, based on the absence of sulfur in bulk and XPS-based elemental analyses, absence of pheomelanin-related features in FTIR & Raman spectra, and the absence of TTCA is AHPO-HPLC analysis of BSF eumelanin.

(2) The solution-based UV-Vis spectra appears consistent with eumelanin, and the A_{650}/A_{500} ratio analysis is consistent with eumelanin containing DHICA.

(3) Both Raman and FTIR peak analysis include COOH moieties, consistent with DHICA monomers being present.

(4) The AFM exhibits a morphology consistent with other natural eumelanins known to contain DHICA. The AFM is also consistent with the DLS measurements, and the zeta potential obtained is consistent with carboxylic groups, which are present in DHICA.

(5) The XPS high-resolution C1s fit indicates some COOH content and the elemental analysis indicates a material intermediate between DHI and DHICA, *i.e.*, BSF eumelanin is consistent in exhibiting probable DHICA content.

(6) The AHPO-HPLC analysis, designed to decompose eumelanin into marker molecules associated with DHI and DHICA (PDCA and PTCA), shows results that are consistent with a material containing both DHI and DHICA when the ratio of these markers are compared. This ratio does not show diminished evidence of DHICA on washing with HCl (designed to remove residual protein).

(7) The NMR data indicates a material system with a higher signal ratio in the carboxyl region *vs.* aromatic region when compared to a synthetic material, the latter of which is well known to be DHICA poor (~5–10%). Therefore, the NMR suggests that BSF eumelanin has DHICA present, potentially in greater quantity than synthetic analogues.

Overall, these data are consistent with the presence of DHICA in BSF eumelanin. We note the use of a different extraction protocol to that of Barek *et al.* However, our use of NaOH is common, and we find no published precedent suggesting our unexpected observations may arise from our approach. The unexpected result of DHICA presence raises questions about its potential origin. One possibility is that BSF eumelanin is produced initially as a poly-DHI system, which through the various refinement processes has oxidized to yield a material with the above properties. Ring fission is possible,[3] but would be inconsistent with the observed AHPO results. Alternatively, BSF eumelanin may be produced by a pathway including DHICA, differing from what is thought to be known of other fly species.[102] These results may vindicate the caution expressed by Sugumaran & Barek.

If BSF eumelanin biosynthesis differs from that in other species, this raises some interesting biological questions, particularly on whether the enzyme needed to produce DHICA within the synthesis pathway is present within the black soldier fly. Furthermore, if the black soldier fly does lack the usual enzyme for producing DHICA, then there may be another, unexplored mechanism producing DHICA-containing eumelanins. Answering these questions may have more general implications for the synthesis and biosynthesis of DHICA-containing eumelanin materials, beyond the black soldier fly.

The presence of DHICA within BSF eumelanin has significant material implications. As has been shown by others, the presence of DHICA within a eumelanin polymer changes not only its morphology, but also its redox properties, making DHICA-rich eumelanin polymers excellent radical scavengers.[6] Furthermore, the DHI-only materials are expected to be more tightly stacked, and thus able to exclude water more efficiently from their internal structures.[6,7,113–115] We therefore infer that this black soldier fly eumelanin would be a promising candidate to exploit the hydration-dependent properties for material applications for which eumelanin is known. In fact, recent papers investigated the hydration/dependent BSF eumelanin electrical properties and found the material very sensitive to hydration changes, in a fashion similar to that observed in synthetic eumelanin.[116] Also, BSF eumelanin was implemented as the active material in fast, responsive humidity sensors[117] and capacitors,[118] which makes BSF eumelanin a competitive and sustainable alternative to other similar materials.

Table 4 Re-normalized signal areas in ^{13}C CP/MAS NMR spectra. The signal area normalized to the eumelanin content in each sample

Sample	Aromatic A (95–140 ppm)	Aromatic B (140–155 ppm)	Carboxyl (160–190 ppm)
BSF eumelanin	0.48	0.13	0.39
Synthetic eumelanin	0.59	0.19	0.22

4. Conclusion

Eumelanin research – and potential applications – have historically been limited by its high cost, low availability and poor

solubility. BSF farming offers a new, sustainable, potentially low-cost and abundant supply of water-processable eumelanin. Here, we have presented a wide range of characterisations of BSF eumelanin. Our data is consistent with the presence of both DHI and DHICA in this material, in contrast to the previous belief that insect eumelanin lacks DHICA. This inconsistency raises intriguing questions about melanogenesis in black soldier flies. In addition, the presence of DHICA in BSF eumelanin has implications for its material applications.

Author contributions

A. B. M.: conceptualization; formal analysis (solid state UV-Vis); investigation (solid state UV-Vis); validation (XPS); writing – original draft preparation; writing – review and editing. S. M.: investigation (AFM, Raman, FT-IR, XPS); formal analysis (AFM, Raman, FT-IR, XPS); writing – original draft preparation (AFM, Raman, FT-IR, XPS); writing – review and editing. S. L.: investigation (synthesis, AHPO, HPLC, DLS); formal analysis (synthesis, AHPO, HPLC, DLS); visualisation; writing – review and editing. G. P.: investigation (solution UV-Vis); formal analysis (solution UV-Vis). M. L.: investigation (solution UV-Vis); formal analysis (solution UV-Vis). P. F. A.: writing – review and editing; supervision. J. V. P.: formal analysis (solid-state NMR); investigation (solid-state NMR); writing – review and editing. J. V. M. L.: formal analysis (NMR); investigation (NMR); writing – original draft preparation (NMR). C. G. O. G.: writing – review and editing; formal analysis (NMR); investigation (NMR); funding acquisition; supervision. J. W. P.: conceptualization; resources (eumelanin extraction); writing – review and editing. M. M.: writing – review and editing; funding acquisition; supervision. A. J. S.: writing – review and editing; funding acquisition; supervision. R. G.: conceptualization; investigation (AFM, Raman, FT-IR, XPS); formal analysis (AFM, Raman, FT-IR, XPS); writing – original draft preparation (AFM, Raman, FT-IR, XPS); writing – review and editing; funding acquisition; supervision. M. A.: conceptualization; methodology (solid state UV-Vis); supervision; resources.

Data availability

The data supporting this article have been included as part of the ESI.†

Conflicts of interest

There are no conflicts of interest to declare.

Acknowledgements

M. A. acknowledges the CNR-Short Term Mobility program 2021 Prot.0052594/230721. M. A. and P. F. A. acknowledges the Italian Ministry of University and Research (MUR) PONa3_00369 SISTEMA. R. G. and S. M. thanks European Union – NextGenerationEU under the Italian Ministry of University and Research (MUR) National Innovation Ecosystem grant ECS00000041 – VITALITY – Spoke 9. M. M. gratefully acknowledges financial support from the European Union's Horizon 2020 research and innovation programme under the Marie Skłodowska-Curie grant agreement No. 843554. A. J. S. is grateful to The Royal Society for research funding (Research Grant RGS\R2\222385). S. L. has been supported by a studentship from the King's China Scholarship Council. S. L., A. J. S., and M. M. are grateful to King's College, Chemistry, for research facilities. A. B. M. acknowledges this work was supported by the UKRI Research Partnerships Investment Fund through the Centre for Integrative Semiconductor Materials. J. V. P., J. V. M. L. & C. F. O. G. acknowledges that this work was financially supported by São Paulo Research Foundation, FAPESP (grant 2013/07296-2 and 2021/03379-7). J. V. P. acknowledges the support of the São Paulo State University research office (PROPe) postdoctoral fellowship (grant 05/2024). We acknowledge Ms Wei Ling Tan from the Elemental Analysis Laboratory, Department of Chemistry, Faculty of Science, National University of Singapore for the elemental analysis.

References

1 A. B. Mostert, *Polymers*, 2021, **13**, 1670.
2 P. Meredith and T. Sarna, *Pigm. Cell Res.*, 2006, **19**, 572–594.
3 M. d'Ischia, K. Wakamatsu, A. Napolitano, S. Briganti, J. C. Garcia-Borron, D. Kovacs, P. Meredith, A. Pezzella, M. Picardo, T. Sarna, J. D. Simon and S. Ito, *Pigm. Cell Res.*, 2013, **26**, 616–633.
4 S. Ito, K. Wakamatsu, M. d'Ischia, A. Napolitano and A. Pezzella, in *Melanins and Melanosomes*, ed. J. Borovanský and P. A. Riley, Wiley-VCH Verlag GmbH & Co., 2011, ch. 6, pp. 167–185.
5 C.-T. Chen, V. Ball, J. J. de Almeida Gracio, M. K. Singh, V. Toniazzo, D. Ruch and M. J. Buehler, *ACS Nano*, 2013, **7**, 1524–1532.
6 L. Panzella, G. Gentile, G. D'Errico, N. F. Della Vecchia, M. E. Errico, A. Napolitano, C. Carfagna and M. d'Ischia, *Angew. Chem., Int. Ed.*, 2013, **52**, 12684–12687.
7 S. Soltani, S. Sowlati-Hashjin, C. G. Tetsassi Feugmo and M. Karttunen, *J. Phys. Chem. B*, 2022, **126**, 1805–1818.
8 P. Meredith, C. J. Bettinger, M. Irimia-Vladu, A. B. Mostert and P. E. Schwenn, *Rep. Prog. Phys.*, 2013, **76**, 034501.
9 P. Meredith, B. J. Powell, J. Riesz, S. P. Nighswander-Rempel, M. R. Pederson and E. G. Moore, *Soft Matter*, 2006, **2**, 37–44.
10 J. V. Paulin, A. P. Coleone, A. Batagin-Neto, G. Burwell, P. Meredith, C. F. O. Graeff and A. B. Mostert, *J. Mater. Chem. C*, 2021, **9**, 8345–8358.
11 A. B. Mostert, S. Rienecker, M. Sheliakina, P. Zierep, G. R. Hanson, J. R. Harmer, G. Schenk and P. Meredith, *J. Mater. Chem. B*, 2020, **8**, 8050–8060.
12 C. C. Felix, J. S. Hyde, T. Sarna and R. C. Sealy, *J. Am. Chem. Soc.*, 1978, **100**, 3922–3926.
13 M. M. Jastrzebska, H. Isotalo, J. Paloheimo, H. Stubb and B. Pilawa, *J. Biomater. Sci., Polym. Ed.*, 1996, **7**, 781–793.

14 B. Szpoganicz, S. Gidanian, P. Kong and P. Farmer, *J. Inorg. Biochem.*, 2002, **89**, 45–53.
15 Y. Liu, L. Hong, V. R. Kempf, K. Wakamatsu, S. Ito and J. D. Simon, *Pigm. Cell Res.*, 2004, **17**, 262–269.
16 J. D. Hong and J. D. Simon, *Photochem. Photobiol.*, 2006, **82**, 1265–1269.
17 T. Sarna, J. S. Hyde and H. M. Swartz, *Science*, 1976, **192**, 1132–1134.
18 P. A. Abramov, S. S. Zhukov, M. Savinov, A. B. Mostert and K. A. Motovilov, *Phys. Chem. Chem. Phys.*, 2023, **25**, 11601–11612.
19 S. Chio, J. S. Hyde and R. C. Sealy, *Arch. Biochem. Biophys.*, 1980, **199**, 133–139.
20 S. Chio, J. S. Hyde and R. C. Sealy, *Arch. Biochem. Biophys.*, 1982, **215**, 100–106.
21 A. B. Mostert, G. R. Hanson, T. Sarna, I. R. Gentle, B. J. Powell and P. Meredith, *J. Phys. Chem. B*, 2013, **117**, 4965–4972.
22 J. V. Paulin, A. Batagin-Neto, P. Meredith, C. F. O. Graeff and A. B. Mostert, *J. Phys. Chem. B*, 2020, **124**, 10365–10373.
23 J. V. Paulin, A. Batagin-Neto and C. F. O. Graeff, *J. Phys. Chem. B*, 2019, **123**, 1248–1255.
24 M. Al Khatib, J. Costa, M. C. Baratto, R. Basosi and R. Pogni, *J. Phys. Chem. B*, 2020, **124**, 2110–2115.
25 T. Vasileiou and L. Summerer, *PLoS One*, 2021, **16**, e0257068.
26 E. Dadachova, R. A. Bryan, X. Huang, T. Moadel, A. D. Schweitzer, P. Aisen, J. D. Nosanchuk and A. Casadevall, *PLoS One*, 2007, **2**, e457.
27 L. Lyttkens, B. Larsson, H. Göller, S. Englesson and J. Stahle, *Acta Oto-Laryngol.*, 1979, **88**, 61–73.
28 R. M. J. Ings, *Drug Metab. Rev.*, 1984, **15**, 1183–1212.
29 P. Jakubiak, F. Lack, J. Thun, A. Urtti and R. Alvarez-Sánchez, *Mol. Pharmaceutics*, 2019, **16**, 2549–2556.
30 M. M. Jastrzebska, A. Kocot and L. Tajber, *J. Photochem. Photobiol., B*, 2002, **66**, 201–206.
31 A. B. Mostert, B. J. Powell, I. R. Gentle and P. Meredith, *Appl. Phys. Lett.*, 2012, **100**, 093701.
32 A. B. Mostert, S. B. Rienecker, C. Noble, G. R. Hanson and P. Meredith, *Sci. Adv.*, 2018, **4**, eaaq1293.
33 Y. J. Kim, W. Wu, S.-E. Chun, J. F. Whitacre and C. J. Bettinger, *Adv. Mater.*, 2014, **26**, 6572–6579.
34 Y. J. Kim, A. Khetan, W. Wu, S.-E. Chun, V. Viswanathan, J. F. Whitacre and C. J. Bettinger, *Adv. Mater.*, 2016, **28**, 3173–3180.
35 I. S. Kwon, Y. J. Kim, L. Klosterman, M. Forssell, G. K. Fedder and C. J. Bettinger, *J. Mater. Chem. B*, 2016, **4**, 3031–3036.
36 H.-A. Park, Y. J. Kim, I. S. Kwon, L. Klosterman and C. J. Bettinger, *Polym. Int.*, 2016, **65**, 1331–1338.
37 M. R. Powell and B. Rosenberg, *Bioenergetics*, 1970, **1**, 493–509.
38 M. Jastrzebska, H. Isotalo, J. Paloheimo and H. Stubb, *J. Biomater. Sci., Polym. Ed.*, 1995, **7**, 577–586.
39 A. B. Mostert, B. J. Powell, F. L. Pratt, G. R. Hanson, T. Sarna, I. R. Gentle and P. Meredith, *Proc. Natl. Acad. Sci. U. S. A.*, 2012, **109**, 8943–8947.
40 S. B. Rienecker, A. B. Mostert, G. Schenk, G. R. Hanson and P. Meredith, *J. Phys. Chem. B*, 2015, **119**, 14994–15000.
41 A. B. Mostert, *J. Mater. Chem. B*, 2022, **10**, 7108–7121.
42 M. Reali, A. Gouda, J. Bellemare, D. Ménard, J.-M. Nunzi, F. Soavi and C. Santato, *ACS Appl. Bio Mater.*, 2020, **3**, 5244–5252.
43 M. Sheliakina, A. B. Mostert and P. Meredith, *Adv. Funct. Mater.*, 2018, **28**, 1805514.
44 J. V. Paulin, S. Bayram, C. F. O. Graeff and C. C. B. Bufon, *ACS Appl. Bio Mater.*, 2023, **6**, 3633–3637.
45 M. P. da Silva, J. C. Fernandes, N. B. de Figueredo, M. Mulato and C. F. O. Graeff, *AIP Adv.*, 2014, **4**, 037120.
46 Z. Tehrani, S. P. Whelan, B. Mostert, J. V. Paulin, M. M. Ali, E. D. Ahmadi, C. F. O. Graeff, O. J. Guy and D. T. Gethin, *2D Mater.*, 2020, **7**, 024008.
47 J. V. Paulin, L. G. S. Albano, D. H. S. Camargo, M. P. Pereira, B. A. Bregadiolli, C. F. O. Graeff and C. C. B. Bufon, *Appl. Mater. Today*, 2022, **28**, 101525.
48 N. L. Nozella, J. V. M. Lima, R. F. de Oliveira and C. F. D. O. Graeff, *Mater. Adv.*, 2023, **4**, 4732–4743.
49 M. Sheliakina, A. B. Mostert and P. Meredith, *Mater. Horiz.*, 2018, **5**, 256–263.
50 P. Kumar, E. Di Mauro, S. Zhang, A. Pezzella, F. Soavi, C. Santato and F. Cicoira, *J. Mater. Chem. C*, 2016, **4**, 9516–9525.
51 C. J. Bettinger and J. Whitacre, *US Pat.*, 9985320, 2018.
52 Y. J. Kim, W. Wu, S. Chun, J. F. Whitacre and C. J. Bettinger, *Proc. Natl. Acad. Sci. U. S. A.*, 2013, **110**, 20912–20917.
53 M. Muskovich and C. J. Bettinger, *Adv. Healthcare Mater.*, 2012, **1**, 248–266.
54 A. N. Tran-Ly, K. J. De France, P. Rupper, F. W. M. R. Schwarze, C. Reyes, G. Nyström, G. Siqueira and J. Ribera, *Biomacromolecules*, 2021, **22**, 4681–4690.
55 J. M. Gallas, *US Pat.*, 4698374, 1987.
56 J. Dong, J. Sun, W. Cai, C. Guo, Q. Wang, X. Zhao and R. Zhang, *Nanomedicine*, 2022, **41**, 102510.
57 A. Camus, M. Reali, M. Rozel, M. Zhuldybina, F. Soavi and C. Santato, *Proc. Natl. Acad. Sci. U. S. A.*, 2022, **119**, e2200058119.
58 E. S. Bronze-Uhle, A. Batagin-Neto, P. H. P. Xavier, N. I. Fernandes, E. R. de Azevedo and C. F. O. Graeff, *J. Mol. Struct.*, 2013, **1047**, 102–108.
59 E. S. Bronze-Uhle, J. V. Paulin, M. Piacenti-Silva, C. Battocchio, M. L. M. Rocco and C. F. D. O. Graeff, *Polym. Int.*, 2016, **65**, 1339–1346.
60 L. Gao, L. Yang, L. Guo, H. Wang, Y. Zhao, J. Xie and N. Shi, *J. Appl. Biomater. Biomech.*, 2022, **20**, 22808000221124418.
61 The Royal Society, *Theo Murphy Meetings*, 2024, From melanogenesis to melanin technologies, Eastbourne, UK.
62 A. van Huis, *Annu. Rev. Entomol.*, 2013, **58**, 563–583.
63 International Platform of Insects for Food and Feed, The European Insect Sector Today: Challenges, Opportunities and Regulatory Landscape, 2019, IPIFF vision paper on the future of the insect sector towards 2030.

64 Y.-S. Wang and M. Shelomi, *Foods*, 2017, **6**, 91.
65 K. C. Surendra, J. K. Tomberlin, A. van Huis, J. A. Cammack, L.-H. L. Heckmann and S. K. Khanal, *Waste Manage.*, 2020, **117**, 58–80.
66 A. Müller, D. Wolf and H. O. Gutzeit, *Z. Naturforsch., C: J. Biosci.*, 2017, **72**, 351–363.
67 C.-H. Kim, J. Ryu, J. Lee, K. Ko, J.-Y. Lee, K. Y. Park and H. Chung, *Processes*, 2021, **9**, 161.
68 A. Mertenat, S. Diener and C. Zurbrügg, *Waste Manage.*, 2019, **84**, 173–181.
69 J. W. Phua and C. J. H. Ottenheim, *US Pat.*, 11981818, 2024.
70 U. D'Amora, A. Soriente, A. Ronca, S. Scialla, M. Perrella, P. Manini, J. W. Phua, C. Ottenheim, R. Di Girolamo, A. Pezzella, M. G. Raucci and L. Ambrosio, *Biomedicines*, 2022, **10**, 2945.
71 N. Ushakova, A. Dontsov, N. Sakina, A. Bastrakov and M. Ostrovsky, *Biomolecules*, 2019, **9**, 408.
72 R. Kerremans, C. Kaiser, W. Li, N. Zarrabi, P. Meredith and A. Armin, *Adv. Opt. Mater.*, 2020, **8**, 2000319.
73 D. Nečas and P. Klapetek, *Open Phys.*, 2012, **10**, 181–188.
74 C. A. Schneider, W. S. Rasband and K. W. Eliceiri, *Nat. Methods*, 2012, **9**, 671–675.
75 N. Fairley, V. Fernandez, M. Richard-Plouet, C. Guillot-Deudon, J. Walton, E. Smith, D. Flahaut, M. Greiner, M. Biesinger, S. Tougaard, D. Morgan and J. Baltrusaitis, *Appl. Surf. Sci. Adv.*, 2021, **5**, 100112.
76 J. V. Paulin, J. D. McGettrick, C. F. O. Graeff and A. B. Mostert, *Surf. Interfaces*, 2021, **24**, 101053.
77 K. Wakamatsu and S. Ito, *Int. J. Mol. Sci.*, 2023, **24**, 8305.
78 S. Ito and K. Fujita, *Anal. Biochem.*, 1985, **144**, 527–536.
79 S. Ito and K. Wakamatsu, *Pigm. Cell Res.*, 1998, **11**, 120–126.
80 P. Meredith and J. Riesz, *Photochem. Photobiol.*, 2004, **79**, 211–216.
81 M. Al Khatib, M. Harir, J. Costa, M. C. Baratto, I. Schiavo, L. Trabalzini, S. Pollini, G. M. Rossolini, R. Basosi and R. Pogni, *Molecules*, 2018, **23**, 1916.
82 N. Madkhali, H. R. Alqahtani, S. Al-Terary, A. Laref and A. Hassib, *Opt. Quantum Electron.*, 2019, **51**, 227.
83 V. Capozzi, G. Perna, P. Carmone, A. Gallone, M. Lastella, E. Mezzenga, G. Quartucci, M. Ambrico, V. Augelli, P. F. Biagi, T. Ligonzo, A. Minafra, L. Schiavulli, M. Pallara and R. Cicero, *Thin Solid Films*, 2006, **511–512**, 362–366.
84 T. Ligonzo, M. Ambrico, V. Augelli, G. Perna, L. Schiavulli, M. A. Tamma, P. F. Biagi, A. Minafra and V. Capozzi, *J. Non-Cryst. Solids*, 2009, **355**, 1221–1226.
85 C. Xin, J.-h Ma, C.-j Tan, Z. Yang, F. Ye, C. Long, S. Ye and D.-b Hou, *J. Biosci. Bioeng.*, 2015, **119**, 446–454.
86 H. Ozeki, S. Ito, K. Wakamatsu and A. J. Thody, *Pigm. Cell Res.*, 1996, **9**, 265–270.
87 K. Wakamatsu and S. Ito, *Pigm. Cell Res.*, 2002, **15**, 174–183.
88 I.-E. Pralea, R.-C. Moldovan, A.-M. Petrache, M. Ilies, S.-C. Heghes, I. Ielciu, R. Nicoara, M. Moldovan, M. Ene, M. Radu, A. Uifalean and C.-A. Iuga, *Int. J. Mol. Sci.*, 2019, **20**, 3943.
89 T. Itou, S. Ito and K. Wakamatsu, *Int. J. Mol. Sci.*, 2019, **20**, 3739.
90 A. Pezzella, M. d'Ischia, A. Napolitano, A. Palumbo and G. Prota, *Tetrahedron*, 1997, **53**, 8281–8286.
91 S. Ito, A. Pilat, W. Gerwat, C. M. B. Skumatz, M. Ito, A. Kiyono, A. Zadlo, Y. Nakanishi, L. Kolbe, J. M. Burke, T. Sarna and K. Wakamatsu, *Pigm. Cell Melanoma Res.*, 2013, **26**, 357–366.
92 D. Niyonkuru, A. Camus, M. Reali, Z. Gao, D. M. Shadrack, O. Butyaev, M. Surtchev and C. Santato, *Nanoscale Adv.*, 2023, **5**, 5295–5300.
93 A. Mbonyiryivuze, Z. Y. Nuru, B. D. Ngom, B. Mwakikunga, S. M. Dhlamini, E. Park and M. Maaza, *Am. J. Nanomater.*, 2015, **3**, 22–27.
94 S. A. Centeno and J. Shamir, *J. Mol. Struct.*, 2008, **873**, 149–159.
95 M. L. Roldán, S. A. Centeno and A. Rizzo, *J. Raman Spectrosc.*, 2014, **45**, 1160–1171.
96 G. Perna, M. Lasalvia, C. Gallo, G. Quartucci and V. Capozzi, *Open Surf. Sci. J.*, 2013, **5**, 1–8.
97 G. Perna, M. Lasalvia and V. Capozzi, *Polym. Int.*, 2016, **65**, 1323–1330.
98 Z. V. Bedran, S. S. Zhukov, P. A. Abramov, I. O. Tyurenkov, B. P. Gorshunov, A. B. Mostert and K. A. Motovilov, *Polymers*, 2021, **13**, 4403.
99 V. Stanic, F. C. B. Maia, R. D. O. Freitas, F. E. Montoro and K. Evans-Lutterodt, *Nanoscale*, 2018, **10**, 14245–14253.
100 I. Galván, A. Jorge, K. Ito, K. Tabuchi, F. Solano and K. Wakamatsu, *Pigm. Cell Melanoma Res.*, 2013, **26**, 917–923.
101 M. Abbas, F. D'Amico, L. Morresi, N. Pinto, M. Ficcadenti, R. Natali, L. Ottaviano, M. Passacantando, M. Cuccioloni, M. Angeletti and R. Gunnella, *Eur. Phys. J. E: Soft Matter Biol. Phys.*, 2009, **28**, 285–291.
102 H. Barek, M. Sugumaran, S. Ito and K. Wakamatsu, *Pigm. Cell Melanoma Res.*, 2018, **31**, 384–392.
103 S. Ito, S. Miyake, S. Maruyama, I. Suzuki, S. Commo, Y. Nakanishi and K. Wakamatsu, *Pigm. Cell Melanoma Res.*, 2018, **31**, 393–403.
104 S. Ito, Y. Nakanishi, R. K. Valenzuela, M. H. Brilliant, L. Kolbe and K. Wakamatsu, *Pigm. Cell Melanoma Res.*, 2011, **24**, 605–613.
105 Y. Liu, L. Hong, K. Wakamatsu, S. Ito, B. Adhyaru, C.-Y. Cheng, C. R. Bowers and J. D. Simon, *Photochem. Photobiol.*, 2005, **81**, 135–144.
106 S. Ghiani, S. Baroni, D. Burgio, G. Digilio, M. Fukuhara, P. Martino, K. Monda, C. Nervi, A. Kiyomine and S. Aime, *Magn. Reson. Chem.*, 2008, **46**, 471–479.
107 B. B. Adhyaru, N. G. Akhmedov, A. R. Katritzky and C. R. Bowers, *Magn. Reson. Chem.*, 2003, **41**, 466–474.
108 P. Thureau, F. Ziarelli, A. Thévand, R. W. Martin, P. J. Farmer, S. Viel and G. Mollica, *Chem. – Eur. J.*, 2012, **18**, 10689–10700.
109 Chem Draw Ultra 12.0.2, *Cambridge Soft Corporation*, 1986-2010.
110 S. Ito and K. Wakamatsu, *Photochem. Photobiol.*, 2008, **84**, 582–592.

111 S. Ito, *Pigm. Cell Res.*, 2003, **16**, 230–236.
112 M. Sugumaran and H. Barek, *Int. J. Mol. Sci.*, 2016, **17**, 1753.
113 M. d'Ischia, A. Napolitano, V. Ball, C. T. Chen and M. J. Buehler, *Acc. Chem. Res.*, 2014, **47**, 3541–3550.
114 P. A. Abramov, O. I. Ivankov, A. B. Mostert and K. A. Motovilov, *Phys. Chem. Chem. Phys.*, 2023, **25**, 16212–16216.
115 S. Soltani, A. Roy, A. Urtti and M. Karttunen, *Mater. Adv.*, 2024, **5**, 5494–5513.
116 M. Ambrico, A. B. Mostert, P. F. Ambrico, J. Phua, S. Mattiello and R. Gunnella, *J. Phys. D: Appl. Phys.*, 2024, **57**, 265303.
117 P. Krebsbach, M. Rincón-Iglesias, M. Pietsch, C. Henel, S. Lanceros-Mendez, J. W. Phua, M. Ambrico and G. Hernandez-Sosa, *ACS Appl. Mater. Interfaces*, 2024, **16**, 42555–42565.
118 N. Al-Shamery, X. Gong, C. Dosche, A. Gupta, M. W. M. Tan, J. W. Phua and P. S. Lee, *Commun. Mater.*, 2024, **5**, 156.